



**Electrical characterization of SnO 2 : Sb ultrathin films obtained by controlled thickness deposition**

Tania R. Giraldi, Alexandre J. C. Lanfredi, Edson R. Leite, Marcia T. Escote, Elson Longo, José A. Varela, Caue Ribeiro, and Adenilson J. Chiquito

Citation: *Journal of Applied Physics* **102**, 034312 (2007); doi: 10.1063/1.2764003

View online: <http://dx.doi.org/10.1063/1.2764003>

View Table of Contents: <http://scitation.aip.org/content/aip/journal/jap/102/3?ver=pdfcov>

Published by the [AIP Publishing](#)

---



## Re-register for Table of Content Alerts

Create a profile.



Sign up today!



## Electrical characterization of SnO<sub>2</sub>:Sb ultrathin films obtained by controlled thickness deposition

Tania R. Giraldi, Alexandre J. C. Lanfredi, and Edson R. Leite  
 LIEC, UFSCar, São Carlos, Brazil, Rod. Washington Luiz, Km 235, 13565-905, São Carlos,  
 São Paulo, Brazil

Marcia T. Escote  
 Universidade Federal do ABC, Santo André, Brazil, Rua Catequese, 240, 09090-400, Santo André,  
 São Paulo, Brazil

Elson Longo and José A. Varela  
 LIEC, UNESP, Araraquara, Brazil, Rua Francisco Degni, s/n, 14800-900, Araraquara, São Paulo, Brazil

Caue Ribeiro<sup>a)</sup>  
 EMBRAPA Instrumentação Agropecuária, São Carlos, Brazil, Rua XV de Novembro, 1452, 13560-970,  
 CP 741, São Carlos, São Paulo, Brazil

Adenilson J. Chiquito  
 Departamento de Física, UFSCar, São Carlos, Brazil, Rod. Washington Luiz, km 235 13565-905,  
 São Carlos, São Paulo, Brazil

(Received 22 February 2007; accepted 19 June 2007; published online 14 August 2007)

A representative study is reported on the electrical properties of SnO<sub>2</sub>:Sb ultrathin films (thickness of 40–70 nm) produced by a deposition method based on aqueous colloidal suspensions of 3–5 nm crystalline oxides. The results revealed the films' electrical behavior in a range of 10–300 K, showing a strong dependence on dopant incorporation, with minimum resistivity values in 10 mol % of Sb content. All the samples displayed semiconductor behavior, but the transport mechanism showed a strong dependence on thickness, making it difficult to fit it to well-known models. In thicker films, the mechanism proved to be an intermediary system, with thermally activated and hopping features. Electron hopping was estimated in the range of 0.4–1.9 nm, i.e., in the same order as the particle size. © 2007 American Institute of Physics.

[DOI: [10.1063/1.2764003](https://doi.org/10.1063/1.2764003)]

### I. INTRODUCTION

In recent years, considerable effort has been dedicated to research on antimony-doped tin oxide (SnO<sub>2</sub>:Sb) due its potential application as a transparent conductor for liquid crystal displays (LCDs) or solar cells. Also, its high reflectivity in the infrared region (due to the plasmon effect) renders SnO<sub>2</sub>:Sb a candidate material for heat-reflective coatings on glass windows and similar applications. In this context, the material is of high technological interest.

One of the main goals in this research effort is the enhancement of the electrical and optical properties of SnO<sub>2</sub>:Sb films by reducing and/or controlling the particle size, deposition, and annealing conditions.<sup>1–6</sup> The literature reports this system as semiconductorlike<sup>7,8</sup>; several authors studied the SnO<sub>2</sub>:Sb electrical properties at room temperature,<sup>1–5,9</sup> reporting resistivity values around 10<sup>-3</sup> Ω cm in films with thickness from 100 to 1280 nm. At room temperature (≈300 K), the scattering mechanism in these SnO<sub>2</sub>:Sb thin films has been attributed to ionized scattering.<sup>4,10</sup> Conversely, below this temperature, some researchers have proposed an activated conduction mechanism for the  $\rho(T)$  curves in measurements between 80–400 K. Based on measurements of film resistivity, Kojima *et al.*<sup>11</sup>

proposed (for 80–330 K range) a temperature dependence in the electronic conduction mechanism; in undoped polycrystalline films, the electron transport mechanism was dominated by the band conduction while in amorphous Sb-Sn-O films this mechanism was governed by the variable-range hopping.

In a previous work,<sup>12</sup> we analyzed the electrical resistivity versus temperature of SnO<sub>2</sub>:Sb films obtained by the polymeric precursor method, and observed two different conduction mechanisms in the temperature range of 10–300 K, i.e., the hopping mechanism and activated conduction. However, that particular study involved films with thicknesses of 300–1000 nm. Recently, we reported a deposition method to produce SnO<sub>2</sub>:Sb ultrathin films,<sup>6</sup> based on another previous work.<sup>13</sup> The procedure, called controlled thickness deposition, was based on a chemical route for the preparation of SnO<sub>2</sub>:Sb nanocrystals at room temperature, resulting in colloidal suspensions whose viscosity was controlled for adequate film deposition. The method allowed for the production of ultrathin and thin films with low resistivity, high transparency, and low roughness, which are important features in electro-optical applications. Although the literature contains several reports about the production of SnO<sub>2</sub>:Sb thin films,<sup>1–5</sup> the main difference reported in this work is layer-by-layer (LbL) control of the film thickness, which al-

<sup>a)</sup>Electronic mail: caue@cnpdia.embrapa.br

lows for the production of ultrathin films with electrical properties similar to those produced in other studies.<sup>6</sup>

Pursuant to the initial study reported earlier,<sup>6</sup> a detailed analysis of the electrical properties of ultrathin films is necessary. Therefore, this article discusses the transport mechanisms in SnO<sub>2</sub>:Sb thin films obtained by this processing method,<sup>13</sup> applying temperatures ranging from 10 to 300 K. To examine the dependence of electrical resistivity ( $T$ ) on temperature, films with different Sb:Sn molar ratios were analyzed. This study involved films with thicknesses of 40–70 nm.

## II. EXPERIMENT

The experiment for producing SnO<sub>2</sub>:Sb nanocrystals has been described in detail elsewhere.<sup>6,14</sup> To produce SnO<sub>2</sub>:Sb nanocrystals, tin (II) chloride dihydrate (SnCl<sub>2</sub>·2H<sub>2</sub>O—Mallinckrodt Baker, USA, purity >99.9%) was dissolved in absolute ethanol at room temperature (tin concentration of 0.025 mol/L). Antimony (III) chloride (SbCl<sub>3</sub> Aldrich, purity 99.9%) solution was prepared similarly. To produce SnO<sub>2</sub>:Sb colloidal suspensions with different antimony contents, the solutions previously prepared were mixed in different molar proportions: 5, 10, 14, and 18 mol % Sb. Under constant stirring, water was added to the mixture of ethanol solutions to promote a reaction of hydrolysis and polycondensation. The product of this reaction was a turbid white suspension, whose pH was kept at approximately 8 by adding NH<sub>4</sub>OH. The Cl<sup>-</sup> ions were removed from the solution by dialyzing it while controlling its pH. The final product consisted of a clear colloidal suspensions of nanocrystalline SnO<sub>2</sub>:Sb. The colloidal suspensions were heated in a glass reactor under constant stirring at a temperature of approximately 70 °C until 90% of the solvent's volume had evaporated.

For the deposition, a few drops of the colloidal suspensions were placed on the substrate, which was then spun in a spin coater (Headway Research, Inc. 1-EC101DT-R790) at 7000 rpm for 30 s. After each layer was deposited, the substrate was dried on a hot plate (≈50 °C) for a few seconds. To reach the desired thickness (40–70 nm), 10 layers were deposited. These films were then heat-treated at 500 °C for 2 h, using a heating and cooling schedule of 5 °C/min.

For the TEM/HRTEM analysis, a drop of the colloidal suspension was deposited on a carbon-covered copper grid. A JEOL 3010 ARP microscope was used for the HRTEM analysis, operating at an acceleration voltage of 300 kV. A TEM-EELS analysis was carried out in a LEO 912 microscope with integrated OMEGA-type imaging spectrometer, operating at an acceleration voltage of 120 kV. The thin film surface morphology was characterized by atomic force microscopy (AFM) (Digital Instruments-Nanoscope III-A).

The electrical resistivity was measured by the usual four point technique. The electrical contacts were defined by shadow masks and standard lithographic techniques. The metallization (In, 100 nm) was carried out in a high vacuum chamber (10<sup>-6</sup> Torr), after which the devices were annealed in an inert Ar atmosphere at 400 °C for 10 min. The electrical measurements were taken using a standard ac lock-in low

frequency (13 Hz) system (AMETEK 7265) or a dc detection apparatus. The current in all experiments was limited to the range of 1–10 μA and, for the temperature-dependent experiments, the samples were placed in a modified Janis CCS 150 closed cycle cryostat.

## III. RESULTS AND DISCUSSION

Figure 1(a) shows the HRTEM measurements in the colloidal suspension. The particles were homogeneous and nanometric, and the estimated average particle size was in the range 3–5 nm. The surface morphology of SnO<sub>2</sub>:10 mol % Sb films was examined by AFM [Fig. 1(b)], which revealed a grain size of ≈13 nm, suggesting that the Sb dopant probably affected the particle-particle interactions, since the average grain size in pure SnO<sub>2</sub> films was approximately 20 nm.<sup>6</sup> Hence, the formation of smaller grains may be related to the substitution of Sb in SnO<sub>2</sub>:Sb thin films.<sup>4</sup> The measured grain size was not correlated with particle size but with the arrangement of the particles on the surface (agglomerates and aggregates). The packing values were estimated at around 0.60, indicating poor packing with these deposition parameters, although these values are higher than those obtained through other techniques, such as the polymeric precursor method.<sup>15</sup>

The incorporation of Sb into the SnO<sub>2</sub> lattice was characterized by electron energy loss spectroscopy (EELS). Figures 1(c) and 1(d) show, respectively, the EELS maps for Sn and Sb elements, indicating the homogeneous distribution of both elements. The Sb map matches the Sn map well, suggesting the incorporation of the former element into the SnO<sub>2</sub> lattice. This assumption is corroborated by the absence of Sb segregation. These results confirm that the chemical method described herein allowed Sb-doped SnO<sub>2</sub> nanoparticles to be synthesized with a high degree of chemical homogeneity.

Figure 2 shows electrical resistivity measurements  $\rho(T)$  as a function of the temperature for SnO<sub>2</sub>:Sb thin films with different Sb molar ratios. The data revealed a clear increase in  $\rho(T)$  values with decreasing temperature in all samples, indicating a semiconductorlike behavior, as expected and observed in the inset for SnO<sub>2</sub>:10% Sb film. In fact, the same behavior was observed in  $\rho(T)$  curves of similar thin films reported in the literature.<sup>7,8</sup>

The absolute resistivity behavior with the doping content exhibited an initial decrease with Sb concentration of up to 10% mol, increasing with concentrations equal to or higher than 14% mol, but showing an optimal behavior with a 10% mol content. This aspect has been observed in others works,<sup>2–5,16</sup> with the optimum concentration (in the range 3%–14% mol) dependent on the growth process. The initial decrease in resistivity was attributed to an increase in the carrier concentration as a result of doping, and the further increase of the resistivity was due to increase of traps concentration (resulting from crystal defects) which dominated the carrier concentration above a critical Sb content.<sup>17</sup> Therefore, Sb atoms act as traps rather as donors.

The resistivity behavior was analyzed using samples with 10% mol Sb (with different thicknesses) in order to

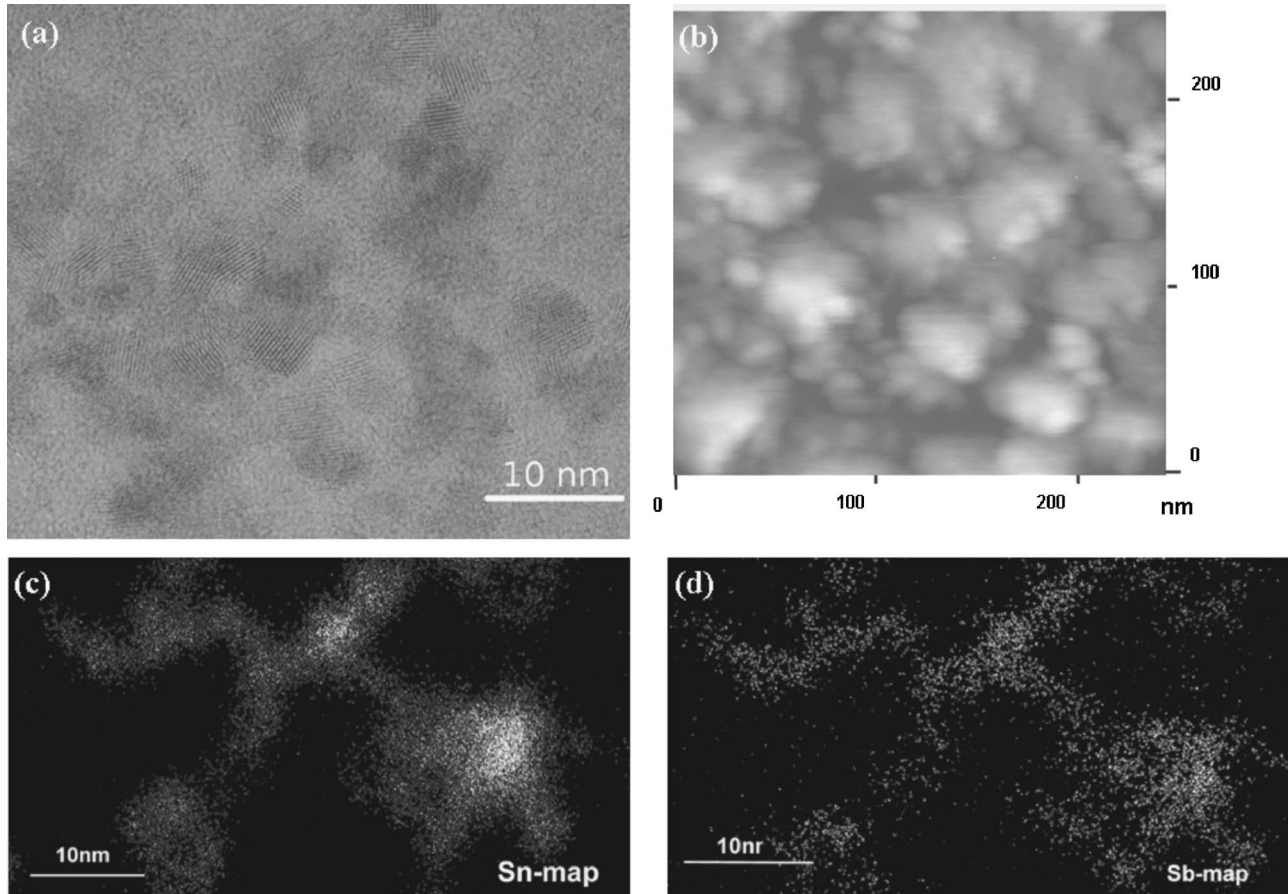


FIG. 1. Morphological characterization of SnO<sub>2</sub>:10% mol Sb: (a) TEM; (b) AFM; (c) EELS pure SnO<sub>2</sub>; and (d) EELS doped SnO<sub>2</sub>

study the dominant electrical transport mechanism. The resistivity data versus temperature were fitted to a generalized model for the activated variable hopping model, in which the electrical resistivity is given by<sup>4</sup>

$$\rho(T) = \rho_0 \exp\left(\frac{T_m}{T}\right)^{1/m}, \quad (1)$$

where  $\rho_0$  is the residual electrical resistivity and  $T_m$  is  $2\alpha^3/k_B \cdot g(E_F)$ . Here,  $g(E_F)$  is the density of states at the Fermi level and  $\alpha^{-1}$  is the localization length.  $m=1$  and 4 correspond, respectively, to the Arrhenius (or thermally acti-

vated) and variable range hopping (VRH) mechanisms. The VRH mechanism normally occurs only in the low temperature region (below room temperature), where the energy is insufficient to excite the charge carrier across the Coulomb gap. Hence, conduction takes place by hopping of small regions ( $k_B T$ ) in the vicinity of the Fermi level where the density of states remains almost constant ( $m=4$ ). This condition is fulfilled when the temperature is sufficiently low or when the energy states are uniformly distributed. Additionally, if one considers the long-range Coulomb interactions, the exponent  $m$  in Eq. (1) should be replaced by 2.<sup>18</sup>

The literature reports that SnO<sub>2</sub>:Sb films display a simple activation mechanism above  $T=100$  K.<sup>12</sup> For the Arrhenius mechanism,  $T_m = E_a/k_B$ .  $E_a$  (activation energy) is usually described as the energy needed to promote the charge carrier across the Coulomb potential between an occupied and an unoccupied site. The best fitting obtained (solid lines in Fig. 2) corresponds to a phenomenological combination of the two above discussed mechanisms, as follows [Eq. (2)]:

$$\rho(T) = \rho_{0,1} \exp\left(\frac{T_{m,1}}{T}\right)^{1/4} + \rho_{0,2} \exp\left(\frac{T_{m,2}}{T}\right). \quad (2)$$

Two good fits were adjusted in the 10 layer film (Fig. 3), corresponding to the 10–60 K and 60–300 K ranges (the data can be seen as two different resistivity measurements taken at distinct temperature ranges). The experimental adjustment therefore shows a greater variation in the conduction mechanism of the 70 nm film than that reported in the literature for

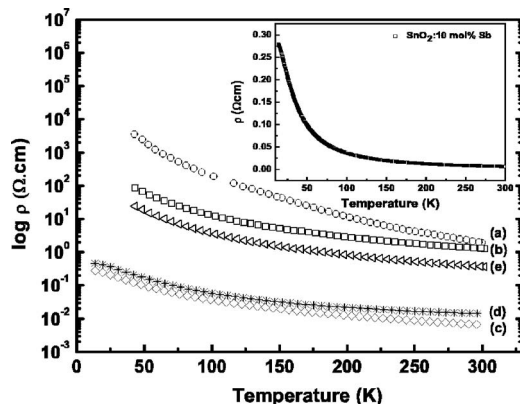


FIG. 2. Resistivity data for different Sb molar concentration. The legend corresponds to Sb contents: (a) 0 (SnO<sub>2</sub> pure); (b) 5%; (c) 10%; (d) 14%; (e) 18%.

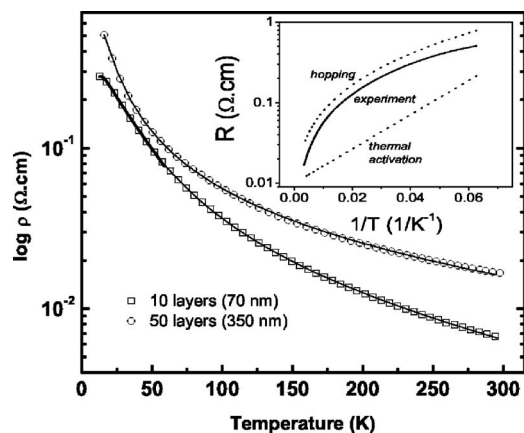


FIG. 3. Resistivity data for different thicknesses (70 nm and 350 nm) in 10% mol dopant concentration. The lines represent the obtained fits for each sample. The thicker line in 70 nm film represents the 10–60 K fitting range, and the thinner line represents the 60–300 K fitting range. The insert shows the individual contribution of hopping and thermal activations mechanisms for the 350 nm film.

thicker films. The fit was better adjusted to the 350 nm film than to the 70 nm, thus indicating a thickness-related dependence. Table I shows the adjusted parameters for each fitting procedure. As can be seen, the contribution of VHR in the 70 nm film was more significant in the range of 10–60 K, as expected. In the 60–300 K range, a very large activation energy (revealed by the parameter  $T_{m,2}$ ) was observed, despite the greater representativeness of this part of the mechanism. This resistivity dependence on the film thickness is probably associated to the influence of the interface film/substrate: as the film thickness decreases it could be expected that superficial roughness or disorder usually present in the substrate becomes more pronounced leading to another scattering mechanism not accounted in our model. In fact could be expected a strong interference of the substrate in a ultrathin film, since the thermal effects are dissipated by the film's large contact surface with the support. It is important to note that other values for the exponent  $m$  (2 and 3) were also used but the results were worse than the presented ones.

The behavior was more regular in the 350 nm film, confirming the interference of thickness. For clearness, the insert shows the individual contributions for hopping and thermal activation mechanisms. On the other hand, the phenomenological adjustment suggests the existence of a particular conduction mechanism probably associated with the nature of the component nanoparticles. Since no sintering / densification processes is expected in SnO<sub>2</sub>-based films produced by the controlled thickness deposition method,<sup>13</sup> we can state

TABLE I. Parameters for phenomenological fitting of resistivity values in SnO<sub>2</sub>:10% Sb films.

	70 nm film		350 nm film
	10–60 K	60–300 K	10–300 K
$\rho_{0,1}$	0.05740	0.00015	0.00140
$T_{m,1}$	964.61	119081.76	24522.05
$\rho_{0,2}$	-0.26383	-0.00408	-0.01050
$T_{m,2}$	13.5967	137.8417	48.9599

that the electron transport will be affected in some way by the interface between particles in the films. Also, these particles can exhibit confinement effects, since the average particle size is close to the Bohr radius for SnO<sub>2</sub> [2.7 nm (Ref. 19)]. Thus, the congruence between Eq. (2) and the resistivity data allowed us to determine the localization length,  $\alpha^{-1}$ . This length can be seen as the distance a carrier moves (hops). If we consider that the energy states  $g(E_F)$  are uniformly distributed, the localization length of the wave function describing the carriers will yield approximately the Bohr radius for the material. Using the sequence proposed by Sato *et al.*<sup>20</sup> to calculate  $g(E_F)$ , and based on the fitting,  $\alpha^{-1}$  is approximately 1.9 nm in 70 nm film (10–60 K), which is comparable with the Bohr radius for SnO<sub>2</sub>, thus confirming the VHR as the dominant mechanism at low temperatures (<60 K).

It is important to note that this fitting procedure provides  $\alpha^{-1} \approx 0.4$  nm in the 70 nm film (60–300 K) and of  $\approx 0.6$  nm in 350 nm film (10–300 K). Despite the differences in the values, the localization lengths in any case are in the same order as the particle sizes. This fact allows us to suggest that the contribution of the particle interfaces is negligible in the VHR mechanism, since the electron hops would be larger than the interference zone caused by the particle boundaries in the film. However, the boundary cannot be negligible in thermally activated processes, since electron transference in those processes is phonon activated. In this case, the dissipation caused by particle packing can strongly affect the transport mechanism, as was observed. In any case, the deviations are greater at higher temperatures.

#### IV. SUMMARY

In summary, we conducted an electrical study of thin and ultrathin SnO<sub>2</sub>:Sb films produced by the controlled thickness deposition method, observing low resistivity values even in ultrathin films. Our results revealed strong interference of the VHR mechanism at low temperatures, which is consistent with the literature. The transport behavior was found to be thickness dependent, an aspect that should be investigated in greater detail in future studies.

#### ACKNOWLEDGMENTS

The authors gratefully acknowledge the financial support of the Brazilian research funding agencies FAPESP and CNPq.

<sup>1</sup>B. Szyszka, S. Jager, J. Szczyrbowski, and G. Brauer, *Surf. Coat. Technol.* **98**, 1304 (1998).

<sup>2</sup>S. Shanthi, C. Subramanian, and P. Ramasamy, *J. Cryst. Growth* **197**, 858 (1999).

<sup>3</sup>E. K. Shokr, *Semicond. Sci. Technol.* **15**, 247 (2000).

<sup>4</sup>C. Terrier, J. P. Chatelon, and J. A. Roger, *Thin Solid Films* **295**, 95 (1997).

<sup>5</sup>M. I. B. Bernardi, L. E. Soledade, I. A. Santos, E. R. Leite, E. Longo, and J. A. Varela, *Thin Solid Films* **405**, 228 (2002).

<sup>6</sup>T. R. Giraldi, C. Ribeiro, M. T. Escote, T. G. Conti, A. J. Chiquito, E. R. Leite, E. Longo, and J. A. Varela, *J. Nanosci. Nanotechnol.* **6**, 3849 (2006).

<sup>7</sup>J. Szanyi, *Appl. Surf. Sci.* **185**, 161 (2002).

<sup>8</sup>J. Rockenberger, U. zum Felde, M. Tischer, L. Troger, M. Haase, and H. Weller, *J. Chem. Phys.* **112**, 4296 (2000).

- <sup>9</sup>D. J. Goyal, C. Agashe, B. R. Marathe, M. G. Takwale, and V. G. Bhide, *J. Appl. Phys.* **73**, 7520 (1993).
- <sup>10</sup>E. Shanthi, V. Dutta, A. Banerjee, and K. L. Chopra, *J. Appl. Phys.* **51**, 6243 (1980).
- <sup>11</sup>M. Kojima, H. Kato, and M. Gatto, *Philos. Mag. B* **73**, 277 (1996).
- <sup>12</sup>T. R. Giraldi, M. T. Escote, A. P. Maciel, E. Longo, E. R. Leite, and J. A. Varela, *Thin Solid Films* **515**, 2678 (2006).
- <sup>13</sup>E. R. Leite, E. J. H. Lee, C. Ribeiro, and E. Longo, *J. Am. Ceram. Soc.* **89**, 2016 (2006).
- <sup>14</sup>E. R. Leite, E. J. H. Lee, T. R. Giraldi, F. M. Pontes, and E. Longo, *J. Nanosci. Nanotechnol.* **4**, 774 (2004).
- <sup>15</sup>T. R. Giraldi, M. T. Escote, M. I. B. Bernardi, V. Bouquet, E. R. Leite, E. Longo, and J. A. Varela, *J. Electroceram.* **13**, 159 (2004).
- <sup>16</sup>S. Y. Lee and B. O. Park, *Thin Solid Films* **510**, 154 (2006).
- <sup>17</sup>A. J. P. Theuwissen and G. J. Declerck, *Thin Solid Films* **121**, 109 (1984).
- <sup>18</sup>N. F. Mott, *Metal-Insulator Transitions* (Taylor and Francis, London, 1974).
- <sup>19</sup>E. J. H. Lee, C. Ribeiro, T. R. Giraldi, E. Longo, E. R. Leite, and J. A. Varela, *Appl. Phys. Lett.* **84**, 1745 (2004).
- <sup>20</sup>T. Sato, K. Ohashi, H. Sugai, T. Sumi, J. Haruna, H. Maeta, N. Matsumoto, and H. Otsuka, *Phys. Rev. B* **61**, 12970 (2000).